Analyst

Accepted Manuscript

ROYAL SOCIETY OF CHEMISTRY

www.rsc.org/analyst

Analyst

RSCPublishing

COMMUNICATION

A Hanging Plasmonic Droplet: Three-Dimensional SERS Hotspots for Highly-Sensitive Multiplex Detection of Amino Acids

uCite this: DOI: 10.1039/x0xx00000x

Received 00th January 2012,
Accepted 00th January 2012

DOI: 10.1039/x0xx00000x

www.rsc.org/

Hongyan Wang,[a] Jinmei Fang,[a] Jifei Xu,[a] Fang Wang,[a] Bai Sun,[b] Shengnan He,[c] Guoping Sun*[a] and Honglin Liu*[b]

A novel and simple platform for efficient SERS detection was demonstrated in a hanging plasmonic droplet of Ag sols by virtue of three-dimensional (3D) SERS hotspots. The platform was a single droplet of concentrated Ag sols with the analytes by hanging itself on a transparent cover glass with hydrophobic treatment. The liquid adhesive force, solvent evaporation, and hydrophobic interaction induced a concentrating of dense nanoparticles into 3D space. The generated 3D hotspots enables highly-sensitive detection of ultratrace analytes and simultaneous multiplex identification of different amino acids, the well-known molecules with low Raman cross sections. This platform demonstrates excellent mechanical stability and is suitable for the excellent examination of ultratrace analytes, with detection limits as low as 0.01 fmol of dye molecules and 5 pmol of amino acids with extremely low Raman cross-sections.

Introduction

Surface-enhanced Raman scattering (SERS) has been widely applied as a powerful analytical technique, which allows ultra-sensitive chemical or biochemical analysis due to remarkable enhancement of many orders of magnitude.[1, 2] However, the performance of SERS depends on many factors, such as the shapes of metallic nanostructures[3], the order degree of SERS substrates[4] and the interaction between molecule and metallic surface[5]. It is necessary to clearly know the origination of large signal enhancements in SERS for finding out simple and efficient strategies to obtain low limit of detection. It has been theoretically and experimentally demonstrated that SERS signals originate from molecules located in nanogaps or clefts, where are called "hotspots". As electromagnetic field is largely enhanced at hotspots, strategies on producing more nanogaps and reducing the distance of nanogaps could maximize the SERS signals and enhance the reproducibility.[6, 7]

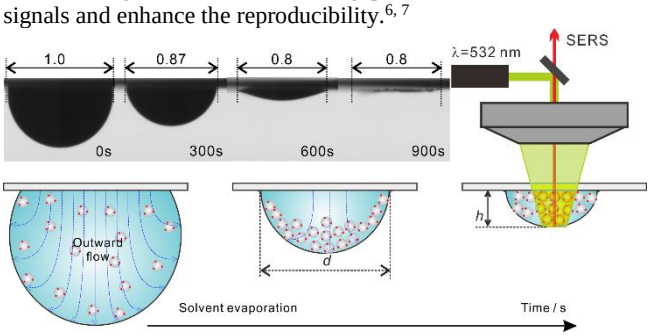

Scheme 1. Illustration of the SERS platform. Top, the photographs of the hanging plasmonic droplet at differnt evaporating stage. The mixed colloidal suspension is hung at the bottom of the quartz glass sheet. The hanging droplets acts as a dynamic substrate for SERS signal collection during the evaporation progress. Bottom, schematic presentation of the fluid flow and particle assembly in the evaporation process. The laser would be located at the centre of the drop and penetrate through quartz glass sheet for successful SERS measurements.

Controlled assemblies of nanoparticles using colloidal chemistry are important for high-yield production of SERS-active nanostructures. Such assemblies placed on two-dimensional solid surfaces have been realized by utilizing electronic[8], ferroelectric[9], thermal[10], mechanical strain[11] or capillary[12] effects. Many strategies have been used to further extend the organiztion of SERS-active colloidal nanopraticles, e.g. synthesis of metallic nanostructures with

different shapes to produce plenty of hotspots[13, 14], fabrication of highly ordered SERS substrates possessing a great many of hotspots.[15] It has been demonstrated that three-dimensional (3D) organization of plasmonic clusters with higher coordination number can generate larger Raman enhancement.[16] Recently, a plasmonic liquid marble by the use of superhydrophobic surface enables simultaneous multiplex SERS identification of ultratrace analytes.[17] However, most reported SERS hotspots have been shown to exist in zero-dimensional point-like, one-dimensional linear, or two-dimensional planar geometries. It remains a formidable challenge to robustly control the orientation and position of nanoparticles in 3D solutions, due to thermal fluctuations and diffusion.[18] We have demonstrated a novel 3D hotspot matrix that can hold hotspots between every two adjacent particles in 3D space, simply achieved by evaporating a droplet of citrate-Ag sols in our earlier work.[19] But how to facilely control the arising of 3D hotspots is affected by many environmental factors, and the answer to utilize the capillary force to stably construct 3D geometry of nanoparticles in 3D solutions is an important research direction in the future.

Herein, we found a novel, simple and efficient method for SERS detection by using hydrophobic surface. In this method, thick silver colloidal suspension with target molecules acting as SERS substrate is dropped onto a piece of hydrophobic quartz glass sheet. The mixed colloidal suspension would be hung at the bottom of the quartz glass sheet, as shown in Scheme 1. The use of a hydrophobic surface prevents the spread of the droplet and keeps the droplet confined as much as possible. The hanging droplets acts as a dynamic substrate for SERS signal collection during the evaporation progress. The laser would be focused at the centre of the drop and penetrate through quartz glass for successful SERS measurements. The process used to dry a hanging droplet can be very beneficial not only for concentrating the analyte and nanoparticles but also preventing the particles from attaching to the edge of the droplet.[20] Influence of droplet drying configuration on SERS performance also indicated a great improvements on hydrophobic surfaces.[21] Therefore, the suspension of a droplet from a hydrophobic surface alters the dynamics in the droplet during evaporation. Three-dimensional (3D) SERS hotspots can be constructed during the detection process. We would collect SERS signals for every second and get the largest signal during the evaporation progress.

Experimental Section

100-fold concentrating of the as-synthesized Ag sols according to classical citrate reduction method was carried out by centrifugation with 10 000 rpm for 10 min. 1 μL of the analyte solution was mixed with 1 μL of the concentrated Ag sols. This 2 μL droplet was dropped on the fluorosilylated quartz silde. The molar numbers mentioned in the following text mean a total volume of 2 μL. Then, the slide was overturned upside down and placed under the 50×objective for SERS measurements. The laser was focused on the bottom of the hanging droplet, i.e. the lower surface of quartz glass sheet. The focal length under our configuration was about 10 μm. The experiments were performed at room temperature. The time-course SERS mapping were recorded under 532 nm laser with 2.5 mW power. Other experimental setups were as follows: the grating of 600 grooves/mm, the exposure time of 1s, the interval period for each spectra of 0.2 s.

Results and discussion

In SERS measurements, larger intensity of signals can be obtained when more molecules are located in hotspots. Different amount of hotspots can be produced by different preparation methods of substrate even using the same colloidal noble metals. The aggregation behaviour of nanoparticles could be guided and the molecules could be forced to hotspot areas by hanging droplets. Usually, there are an outward flow of the solvent from the middle to the edge and this flow will bring particles and molecules to the periphery of droplet (as shown in Scheme 1).[22] The contact area between the drop and the substrate decreases as the drop dries. But only the super-hydrophobic surface can break the diffusion limit.[23] We have illustrated the diameter of the contact area in Scheme 1. It clear showed a withdrawing of the contact line on fluorosilylated surface, but only a decrease of 20% was observed in the final dried state. The drop would be certain to flat out at at some point in the process of the droplet evaporation. Therefore, small and freely suspended nanoparticles and molecules in the droplet are dragged to the droplet periphery and thick aggregations formed along the edge. Although this phenomenon can be weakened on hydrophobic surface, the ring of particle aggregations can't be fully avoided.

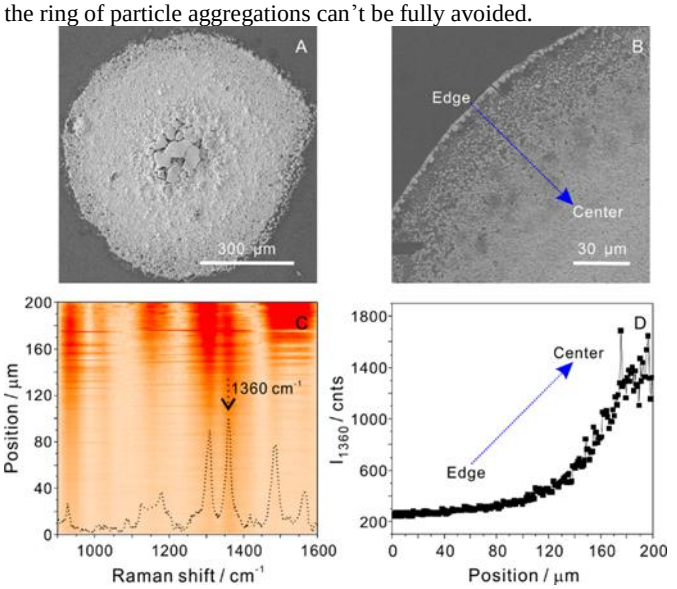

Fig. 1. (A) SEM images of depositions from a suspending droplet drying on hydrophobic quartz glass sheet. B) High magnification SEM images of the deposition shown in Fig. 1A. C) Line SERS mapping in the range of 0-200 μm with R6G molecule numbers of 100 fmol. D) Line SERS mapping measured on the ring formed from a suspending droplet ranging from the edge to the centre. The concentrate of R6G used for this measurement is 100 fmol. The exposure time is 1s and the increment is 1 μm.

Fig. 1 show the particle deposition state of hanging droplet on hydrophobic surface after all the moist water of the drops is exhausted by evaporation. Coffee ring stains would form when the evaporation rate at the solid/liquid/air triple-phase boundary of the droplet is larger than other region of liquid surfaces, which induces a fluid flux toward the contact line to compensate for solvent loss.[24] Consequently, a flow is generated in the evaporating droplet, then more particles are carried to the edge (Fig. 1B).[25] But why most of particles were concentrated in the center of the contact area? In the final stage of evaporation, the sharp increase of the ionic strength and particle concentration produced the 'trapping well' of particle-particle interactions,[19] which induced the aggreating or assembling together of nanoparticles, i.e. the spherical colloidal particles form closely packed aggregates and the ability of interfacial aggregates to resist bulk flow was increased,[26] whereas the particles with a tendency to aggregate and adsorb at the liquid–gas interface,[27] eliminating the coffee-ring effect of large aggregates. As suggested by Yunker et al, the aggregation of nanoparticles affects their shape.[26] And the liquid adhesive force promoted the closely-packed

assembly of the aggregates into the center area. The particles will accumulate at the apex of the overturned droplet. As the solvent volume decreases, nanoparticles will be highly concentrated in the middle of the droplet and they will adhere to the substrate surface after all the water is evaporated. As shown in Fig. 1A, the final products of 1 µl colloidal dispersion drying on hydrophilic surface are typically a round structure with an deposition area of 600 µm in diameter. Besides, aggregations bulge in the middle of the ring and edges have low particle density. To further understand the aggregation behaviour of the nanoparticles, a careful look into the deposition is made by SEM images. Fig. 1B is the high magnification SEM images of the deposition shown in Fig. 1A. It shows typical depositions from the edge to centre of a suspending droplet. It is clearly that the margin of the ring is thicker than other area, the periphery shows lower particle density.

As the amount of hotspots would change with the degree of aggregation and molecules would also distribut nonuniform, different areas would show different SERS enhancement. We studied the changing of peak intensity in the depositions by SERS linear mapping. The edge of the rings were set as original points, then SERS mapping measurements were taken from 0 µm to 200 µm, which were ranging from the edge to the centre. Fig. 1C are peaks changing tendency of all SERS spectrogram measured on the ring formed from a suspending droplet. SERS intensities of 100 fmol R6G at ~1360 cm^{-1} were managed for monitoring intensity change, as shown in Fig. 1D. In the edge area, SERS intensities are about 300 cnt. However, a raising is oberved when approaching the centre and the intensity of signals collected from centre area are about 1800 cnt. By comparison, we find the centrality of the ring formed from a suspending droplet displayed the highest SERS active. More efficient hotspots can be produced along the central axis of a suspending droplet.

Our method has several advantages comparing with conventional SERS methods. First, general materials are used as SERS substrate. The thick silver colloidal suspension is hung and acts as a dynamic substrate. Second, 3D SERS hotspots can be obtained due to the concentrating caused by the volatilization and hydrophobic effect during the detection process.[28] Third, large LSPR would be produced due to capillary force induced desired distance between the nanostructures.[29] Finally, under the protection of solvent, silver nanoparticle substrates can't be oxidized.[12] Hydrophobic surfaces weaken the electrostatic adsorption of nanoparticles, increase the uniformity of deposition, and imporve the sensitivity and reproducibility of SERS signals.[30, 31] Hydrophobic surfaces could not only concentrate nanoparticles to produce a large number of hotspots in a 3D geometry, but also concentrate dissolved solutes in aqueous droplets. Molecules could be concentrated into a small region and more molecules would enter the hotspot areas.

The ideal closely-packed assembly of 2D nanosphere arrays is shown in Fig. S1, and it produces multiple hotspots in a uniform fashion over a large area. Ideally, the total number of hotspots in a 2D array is three times the number of particles (Fig. S1). Therefore, the density of these hotspots is ultimately limited by the 2D plane, but 3D hotspot matrix can greatly increase the number of hotspots.[19] Actually, in dry state, many AgNPs are contained within the aggregates, which induced the sharply decrease of SERS signals (Fig. 2B). When g is smaller than 1 nm, the quantum tunneling arises and dramatically reduces the electromagnetic enhancing ability. Secondly, as the particles touch to each other, the charge exchange phenomena occur, leading to the decay of electric field enhancement. Finally, the solid contacts among particles make the whole aggregate an equipotential body and thus give rise to electrostatic shielding phenomenon which would further decrease the electric field enhancement. Thus many particles, except for the particles on the surfaces, are not available to enhance the SERS signal. Nevertheless, during the drying process of Ag sols, the particle-particle interactions of van der Waals attraction and electrostatic repulsion can create the 'trapping well'[19] for immobilizing particles in 3D space and result in a huge number of hot spots in 3D geometry.

SERS performance of our proposed method was measured using R6G as the probe analyte. One drop of R6G aqueous solutions was dropped onto the quartz glass sheet, then the laser was focused on the centre of the bottom and penetrated through quartz glass sheet, as shown in Scheme 1. The collection time in the SERS time mapping measurement last for 1200 seconds. As shown in Fig. 2A, there exist slow enhancement of the signal at the first several hundred seconds, then the signal enhancd quickly at the following one hundred seconds and finally reached the highest peak. After that, the signal fade rapidly. Fig. 2B is time-course two-dimensional SERS mapping of 1000 fmol R6G at ~1360 cm^{-1}, the result shown that the highest SERS enhancement could be obtained at about 700 seconds. To explore the detection limit of our novel method, a series of low concentratisssons of R6G aqueous solutions ranging from 100 fmol to 0.01 fmol were measured. As shown in Fig. 2C , the highest SERS spectra of R6G with different molecule numbers collected by our method were shown and the minimum detectable molecule nunmbers of our method was 0.01 fmol.

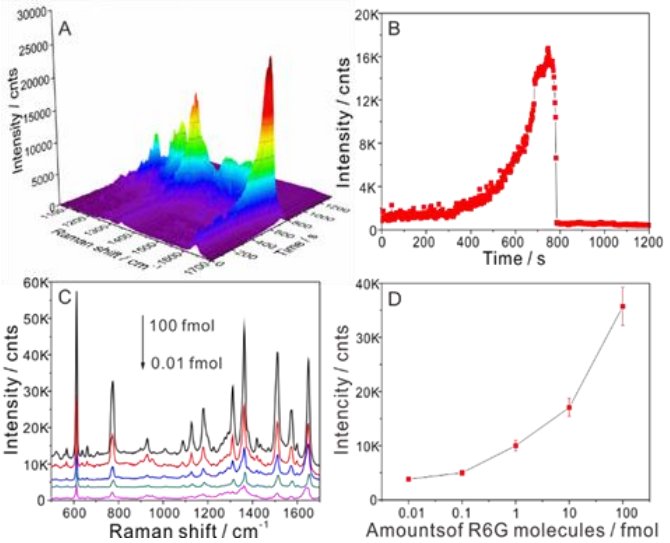

Fig. 2. A) Time-course SERS mapping of 10 fmol R6G in a 2 µl suspending droplet by the use of our SERS platform. B) SERS intensity changing of the 1360 cm^{-1} peak as shown in A. C) Typical SERS spectra of R6G with different moles (from top to bottom): 100, 10, 1, 0.1, 0.01 fmol (these spectra were the ones with the maximal intensity in the time-course mapping). D) The molecule number dependence of the SERS intensity at 1360 cm^{-1}.

Amino acids have extremely low cross-sections for both absorption and Raman scattering and most of them have low affinity to noble metal surface. In order to evidence the capability of our SERS platform by the virtue of 3D hotspots, simultaneous ultratrace detection of amino acids is demonstrated in Fig. 3. The SERS spectrum for the interfacial detection of tyrosine and phenylalanine shows fingerprint peaks corresponding to both probe molecules. The fingerprint SERS peaks of phenylalanine were encoded by the blue bars, and that of tyrosine by the red bars. The results clearly evidenced that the peaks of multiplex spectrum was well fitted by the blue and red bars. A comparison of this SERS spectrum with those for single analyte detection shows that the blue bars can be explicitly indexed to phenylalanine, whereas the red bars can be assigned to tyrosine (Fig. 3). Hence, it is evident that the hanging of

droplet provides an analytical platform for bioassay with SERS signals. Moreover, our platform could be used to successfully detect a variety of amino acids with different chemical features that contained different functional groups, such as the nonpolar groups on valine and phenylalaine, the uncharged polar groups on tyrosine, the positively charged groups on arginine, and the high metal affinity group on cysteine (i.e. thiol groups). Similar experiments have been designed for simultaneous multiplex SERS detection of 0.5 pmol tyrosine-valine (Fig. S2) and 5 pmol cysteine-arginine (Fig. S3). The presence of a thiol, amine, aromatic, heterocycle or nonpolar moiety on the amino acid molecules leads to different binding efficiencies with the metal surface and thus yields different Raman enhancements. The fingerprint pattern of tyrosine dominated the features of multiplex SERS spectrum of 0.5 pmol tyrosine-valine (Fig. S2). This implied that the amino acids with simple side chains (e.g. cysteine, arginine, and valine) generated much weaker SERS signals, compared to the aromatic amino acids (e.g. tyrosine and phenylalaine). A higher molecule number (5 pmol) of cysteine-arginine generated the tolerable signal-to-noise ratios for multiplex SERS detection (Fig. S3). Nevertheless, by the virtue of our 3D hotspots, simultaneous detection of amino acids at μM levels can be easily achieved, and the signal-to-noise ratio and sensitivity were much better than those obtained using dried substrates.

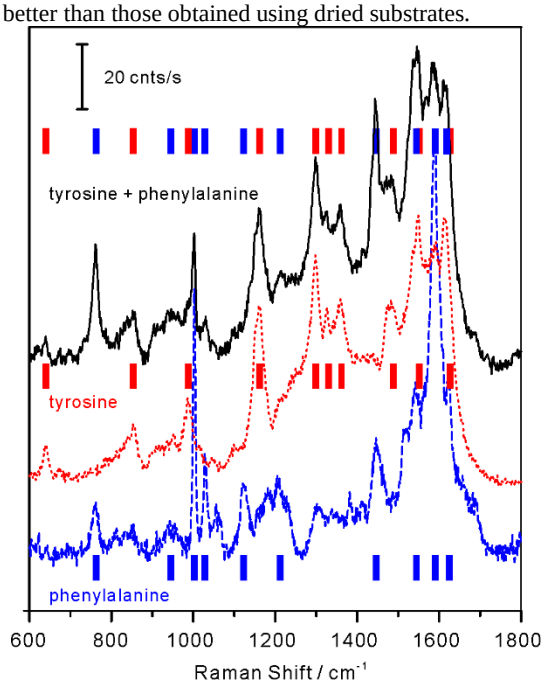

Fig. 3. SERS spectra for the multiplex detection (top) of tyrosine and phenylalaine. Individual SERS spectra of tyrosine in the aqueous phase (middle) and phenylalanine in the aqueous phase (bottom) at the same respective moles (0.5 pmol) are included for comparison.

In this regard, our method provides the capability for practical application. Owing to the hydrophobic condensation effect and the power of liquid adhesive force during evaporation, AgNPs would be highly concentrated at the bottom of the droplet. Besides, it's hard for nanoparticles to deposited on hydrophobic surface, there are no particles deposited on the hydrophobic surface when the drops are not dried, so there are more particles in the drop. As a result, a larger amount of 3D SERS hotspots would be produced and these hotspots would make the largest enhancement when the largest capillary force arised during evaporation.[32] What's more, the R6G solution became more and more concentrated, contributing to the effective delivery of R6G molecules to the hotspot areas at interstitial sites between nanoparticles.[33] The laser coming from the Raman instrument might also affect the nanoparticles assembling and molecule moving in the focused incident laser spot.[34, 35] Moreover, in liquid state, the solvent can protect the target molecules from photobleaching and photodegradation during the state transformation process from wet state to dry state.

Conclusions

Our contribution demonstrated a novel and effective SERS detection method. The accumulation of molecules and AgNPs in the middle of the droplet occurs under the influence of the liquid adhesive force. Under the hydrophobic condensation effect, Ag-NPs could aggregate to produce a lot of 3D SERS hotspots and molecules can be driven to the hotspot areas, which lead to the largest contribution to SERS signals. Here, an efficient laser focus method was developed for effective SERS detection. We focused laser in the middle of the bottom of the hanging droplet, which was also the lower surface of quartz glass sheet. The results indicate that the quality and reproducibility of the SERS spectra from the middle of the droplet is better than other area. A detection limit of down to 0.01 fmol for R-6G can be achieved by suspending the droplet. In all, our method was proved to be an excellent SERS detection method with both high sensitivity and reproducibility. Of course, if the laser can incident from the liquid drop bottom and overcome the quartz glass for laser cut, the signal will be further improved. It could be expected that this method can be practically used for the rapid trace analysis in the near future.

Acknowledgements

This work was supported by the CETC Technological Innovation Fund (JJ-QN-2013-35), National Natural Science Foundation of China (21305142), Natural Science Foundation of Anhui Province (1308085QB27), and Cultivation Project for the NSFC Youth Foundation of the First Affiliated Hospital of Anhui Medical University (2013KJ05).

Notes and references

[a] Department of Oncology, The First Affiliated Hospital of Anhui Medical University, Hefei 230022, P.R. China. E-mail: sungp@ahmu.edu.cn .
[b] Institute of Intelligent Machines, Chinese Academy of Sciences, Hefei 230031, P.R. China. Fax: +86-551-65592420; Tel: +86-551-6559-2385; E-mail: hlliu@iim.ac.cn .
[c] No.38 Research Institute of China Electronics, Technology Group Corporation, Hefei 230088 (P.R. China).

† Electronic Supplementary Information (ESI) available: Experimental details and multiplex SERS detection of six other amino acids. See DOI: 10.1039/c000000x/

1. R. A. Alvarez-Puebla, R. Contreras-Caceres, I. Pastoriza-Santos, J. Perez-Juste and L. M. Liz-Marzan, *Angew. Chem. Int. Ed.*, 2009, **48**, 138-143.
2. M. Rycenga, X. Xia, C. H. Moran, F. Zhou, D. Qin, Z. Y. Li and Y. Xia, *Angew. Chem. Int. Ed.*, 2011, **50**, 5473-5477.
3. Z. Zhu, H. Meng, W. Liu, X. Liu, J. Gong, X. Qiu, L. Jiang, D. Wang and Z. Tang, *Angew. Chem. Int. Ed.*, 2011, **50**, 1593-1596.
4. J. Zeng, Y. Ma, U. Jeong and Y. Xia, *J. Mater. Chem.*, 2010, **20**, 2290.
5. L. F. Zhang, S. L. Zhong and A. W. Xu, *Angew. Chem. Int. Ed.*, 2013, **52**, 645-649.
6. J. C. F. Toledano, F. Sciortino and E. Zaccarelli, *Soft Matter*, 2009, **5**, 2390-2398.
7. H. C. Schniepp, J.-L. Li, M. J. McAllister, H. Sai, M. Herrera-Alonso, D. H. Adamson, R. K. Prud'homme, R. Car, D. A. Saville and I. A. Aksay, *J. Phys. Chem. B*, 2006, **110**, 8535-8539.

8. W. Dickson, G. A. Wurtz, P. R. Evans, R. J. Pollard and A. V. Zayats, *Nano Lett.*, 2008, **8**, 281-286.
9. H. L. Chen, K. C. Hsieh, C. H. Lin and S. H. Chen, *Nanotechnology*, 2008, **19**, 435304.
10. G. Xu, C. M. Huang, M. Tazawa, P. Jin and D. M. Chen, *J. Appl. Phys*., 2008, **104**, 053102.
11. K. D. Alexander, K. Skinner, S. Zhang, H. Wei and R. Lopez, *Nano Lett.*, 2010, **10**, 4488-4493.
12. H. Liu, Y. Sun, Z. Jin, L. Yang and J. Liu, *Chem. Sci.*, 2013, **4**, 3490-3496.
13. J. Zhang, X. Li, X. Sun and Y. Li, *J. Phys. Chem. B*, 2005, **109**, 12544-12548.
14. X. Lu, M. Rycenga, S. E. Skrabalak, B. Wiley and Y. Xia, *Annu. Rev. Phys. Chem.*, 2009, **60**, 167-192.
15. M. Rycenga, J. M. McLellan and Y. Xia, *Chem. Phys. Lett.*, 2009, **463**, 166-171.
16. N. Pazos-Perez, C. S. Wagner, J. M. Romo-Herrera, L. M. Liz-Marzan, F. J. G. de Abajo, A. Wittemann, A. Fery and R. A. Alvarez-Puebla, *Angew. Chem. Int. Edit.*, 2012, **51**, 12688-12693.
17. H. K. Lee, Y. H. Lee, I. Y. Phang, J. Wei, Y.-E. Miao, T. Liu and X. Y. Ling, *Angew. Chem. Int. Edit.*, 2014, **126**, 1-6.
18. K. Kim, H. S. Han, I. Choi, C. Lee, S. Hong, S.-H. Suh, L. P. Lee and T. Kang, *Nat. Commun.*, 2013, **4**.
19. H. Liu, Z. Yang, L. Meng, Y. Sun, J. Wang, L. Yang, J. Liu and Z. Tian, *J. Am. Chem. Soc.*, 2014, **136**, 5332-5341.
20. S. Keskin and M. Culha, *Analyst*, 2012, **137**, 2651-2657.
21. E. Avci and M. Culha, *RSC Adv.*, 2013, **3**, 17829-17836.
22. T. Still, P. J. Yunker and A. G. Yodh, *Langmuir*, 2012, **28**, 4984-4988.
23. F. De Angelis, F. Gentile, F. Mecarini, G. Das, M. Moretti, P. Candeloro, M. L. Coluccio, G. Cojoc, A. Accardo, C. Liberale, R. P. Zaccaria, G. Perozziello, L. Tirinato, A. Toma, G. Cuda, R. Cingolani and E. Di Fabrizio, *Nat. Photonics*, 2011, **5**, 683-688.
24. V. L. Morales, J.-Y. Parlange, M. Wu, F. J. Perez-Reche, W. Zhang, W. Sang and T. S. Steenhuis, *Langmuir*, 2013, **29**, 1831–1840.
25. H. Hu and R. G. Larson, *Langmuir*, 2005, **21**, 3963-3971.
26. P. J. Yunker, T. Still, M. A. Lohr and A. G. Yodh, *Nature*, 2011, **476**, 308-311.
27. M. Anyfantakis and D. Baigl, *Angew. Chem. Int. Edit.*, 2014, **53**, 14077-14081.
28. K. Qian, L. Yang, Z. Li and J. Liu, *J. Raman Spectrosc.*, 2013, **44**, 21-28.
29. L. Yang, H. Liu, Y. Ma and J. Liu, *Analyst*, 2012, **137**, 1547-1549.
30. L. Q. Lu, Y. Zheng, W. G. Qu, A. W. Xu and H. Q. Yu, *J. Mater. Chem.*, 2012.
31. M. Kahraman, B. N. Balz and S. Wachsmann-Hogiu, *Analyst*, 2013, **138**, 2906-2913.
32. B. Gao, T. S. Steenhuis, Y. Zevi, V. L. Morales, J. L. Nieber, B. K. Richards, J. F. McCarthy and J.-Y. Parlange, *Water Resour. Res.*, 2008, **44**, W04504.
33. Z. Guo, X. Chen, J. Li, J. H. Liu and X. J. Huang, *Langmuir*, 2011, **27**, 6193-6200.
34. X. Chen and X. Wang, *J. Phys. Chem. C*, 2011, **115**, 22207-22216.
35. K. W. Adu, H. R. Gutierrez and P. C. Eklund, *Vib. Spectrosc.*, 2006, **42**, 165-175